Supported Information

Unprecedented aluminum molecular ring based layer with tailorable optical limiting effect

Lin Geng,[a#] Di Wang,[b#] Ran-Qi Chen,[a] San-Tai Wang,[a] Chan Zheng,*[b] Jian Zhang[a] and Wei-Hui Fang*[a]

[a] State Key Laboratory of Structural Chemistry, Fujian Institute of Research on the Structure of Matter, Chinese Academy of Sciences, 350002 Fuzhou, P.R. China

[b] Institute of Biology and Chemistry, Fujian University of Technology, 350118 Fuzhou, P.R. China

# These authors contributed equally to this work.

E-mail: fwh@fjirsm.ac.cn

Content

1. Experimental section

1.1 Materials and Characterization Measurements

All the reagents and solvents employed were purchased commercially and used as received without further treatment. Aluminum isopropoxide, cuprous chloride and nicotinic acid (NA) were acquired from Aladdin Chemical Reagent Shanghai. Propanol, 1,4-dioxane (diox), triethylamine, and methylamine were acquired from Sinopharm Chemical Reagent Beijing.

The Fourier transform infrared spectroscopy (FT-IR) data (KBr pellets) was recorded on a PerkinElmer Spectrum 100 FT-IR spectrometer over a range 400-4000 cm^{-1}. PXRD X-ray diffraction (PXRD) data were collected on a Rigaku Mini Flex II diffractometer using CuK radiation ($\lambda = 1.54056$ Å) under ambient conditions. The UV-vis diffuse reflection data were recorded at room temperature using a PXRD sample with $BaSO_4$ as a standard (100 % reflectance) on a Perkin Elmer Lamda-950 UV spectrophotometer and scanned at 200-800 nm. The absorption data are calculated from the Kubelka-Munk function, ($F(R) = (1-R)^2/2R$), where R representing the reflectance. Scanning electron microscopy (SEM; SEM-450) and atomic force microscopy (AFM; HAR1-200-10) were used to investigate the surface characteristic of the MOF nanosheets. Elemental composition was analyzed by X-ray photoelectron spectroscopy (XPS; ESCALAB 250). Ultraviolet–visible spectroscopy (UV–vis; UV-2600) was used to determine the absorption peaks and band gaps of MOF nanosheets. Fluorescence spectroscopy (FLS980) was used to measure excitation and emission spectra.

1.2 Synthesis of H[Al$_8$(NA)$_{12}$(μ-OH)$_4$(OPr^n)$_8$(Cl)]·4(C$_3$H$_7$OH)(H$_2$O) (AlOC-196)

A mixture of aluminum isopropoxide (300 mg, 1.47 mmol), nicotinic acid (200 mg, 1.62 mmol), NaCl (5 mg, 0.09 mmol) and propanol (5 mL) was sealed in a 20 mL vial and transferred to a preheated oven at 100 °C for 5 days. When cooled to room temperature, colorless crystals were obtained. (yield: 47 % based on Al(O^{i}Pr)$_3$). The crystals are rinsed with ethanol and preserved under a sealed and dry environment.

1.3 Synthesis of $[Al_8Cu^{II}Cu^{I}Cl_2(NA)_{12}(\mu\text{-}OH)_4(OPr^n)_8(Cl)]\cdot10(H_2O)$ (AlOC-197)

A mixture of aluminum isopropoxide (300 mg, 1.47 mmol), cuprous chloride (100 mg, 1.01 mmol), nicotinic acid (200 mg, 1.62 mmol), triethylamine (300 μL), 1,4-dioxane (3 mL) and propanol (5 mL) was sealed in a 20 mL vial and transferred to a preheated oven at 100 °C for 5 days. When cooled to room temperature, colorless crystals were obtained. (yield: 53 % based on $Al(O^iPr)_3$). The crystals are rinsed with ethanol and preserved under a sealed and dry environment.

1.4 Synthesis of 2D nanosheets

The **AlOC-197** nanosheets were fabricated by liquid exfoliation. The layered **AlOC-197** bulk crystals (10 mg) was dispersed in deionized water (12 mL) and then treated ultrasonically for 4 h at 280 W and 0 °C by keeping the sample in an ice bath. The obtained suspension was centrifuged at 3000 rpm for 10 min and the supernatant was collected to obtain **AlOC-197** nanosheets.

1.5 X-ray Crystallographic Analyses

Crystallographic data of crystal **AlOC-196** and **AlOC-197** were collected on Super Nova equipped with Cu-Kα radiation (λ = 1. 54184 Å) at about 100 K and 293 K, respectively. The structures were solved with the dual-direct methods using ShelxT and refined with the full-matrix least-squares technique based on F^2 using the *SHELXL*. Non-hydrogen atoms were refined anisotropically. Hydrogen atoms were added theoretically, riding on the concerned atoms and refined with fixed thermal factors. Hydrogen atoms bonded to hydroxyl ions were not located from difference maps or included in the refinement. Besides. All absorption corrections were performed using the multi-scan program. The diffused electron densities resulting from residual solvent molecules were removed from the data set of **AlOC-196** using the *SQUEEZE* routine of *PLATON* and refined further using the data generated.

1.6 Z-Scan Measurements

The NLO responses of the MOFs were evaluated using the Z-scan method with an

Nd:YAG laser with a repetition rate of 10 Hz as the excitation light source. The laser pulses (period: 7 ns; wavelength: 532 nm) were separated into two beams with a mirror. The pulse energy at the front and back of the samples was monitored using an energy detector. All measurements were taken at room temperature. Each sample was mounted on a computer-controlled translation stage that moved the sample along the z-axis.

1.7 NLO properties

To quantify the NLO properties of the **AlOC-197** nanosheets, the nonlinear absorption coefficients were determined using an RSA model. The total absorption coefficient $\alpha(I)$ can be denoted as:

$$\alpha(I) = \frac{\alpha_0}{1 + I/I_S} + \beta I \tag{1}$$

where α_0 is the linear absorption coefficient, I_S is the saturable intensity, and β is the nonlinear absorption coefficient. Therefore, the modified normalized transmittance T can be denoted as:

$$T = \frac{1}{\sqrt{\pi}\left[\frac{\beta I_0 L_{eff}}{(1+z^2/z_0^2)}\right]} \int_{-\infty}^{+\infty} \ln\left[1 + \frac{\beta I_0 L_{eff}}{(1+z^2/z_0^2)} \exp(-t^2)\right] dt \tag{2}$$

where I_0 is the peak intensity of the input laser beam at the focal point, z_0 is the Rayleigh diffraction length of the laser beam calculated through $z_0 = \pi \omega_0^2/\lambda$, and λ is the wavelength of the incident light. Additionally, $L_{eff} = (1 - e^{-\alpha_0 L})/\alpha_0$ is the effective thickness of the sample, where α_0 is the linear absorption coefficient and L is the sample thickness. The imaginary part of the third-order NLO susceptibility, $Im\chi^{(3)}$, is directly related to β by:

$$Im\chi^{(3)} = \left[\frac{10^{-7} c\lambda n^2}{96\pi^2}\right] \cdot \beta \tag{3}$$

where c is the speed of light and n is the refractive index. From the fitting of Z-scan curves, we derived NLO parameters related to nonlinear absorption, including β, $Im\chi^{(3)}$, and FOM of the **AlOC-197** nanosheets, which are listed in Table S4. To evaluate the NLO performance of the as-prepared **AlOC-197** nanosheets, we also summarize the relevant NLO parameters for other low-dimensional materials in Table S5, along with experimental conditions. As seen from Table S5, the NLO parameters obtained in the present study are similar or better than reported values for $MoSe_2$ nanosheets, Sb nanosheets, GeSe nanosheets, SnSe nanosheets, BN nanosheets and CuS nanosheets. Therefore, these ecofriendly **AlOC-197** nanosheets are a promising material for use in photonic devices.

2. Detailed coordination environment information for 0D aluminum molecular ring AlOC-196
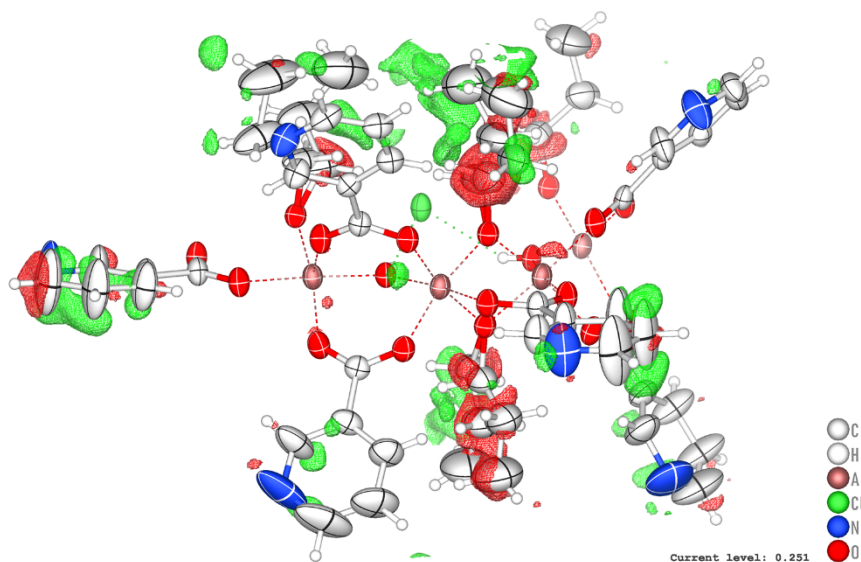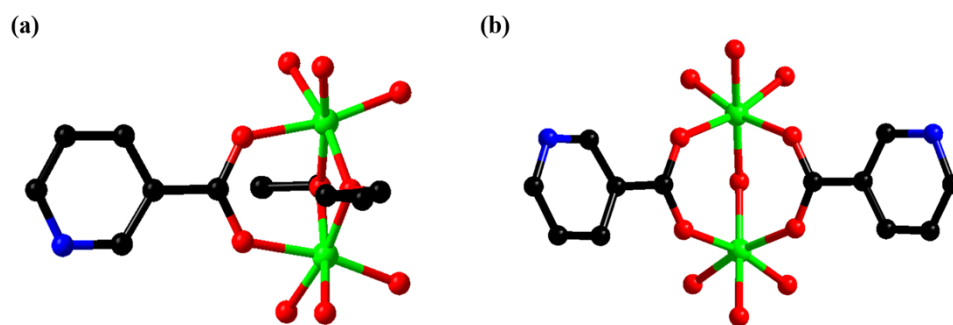

Fig. S1. Thermal ellipsoid diagram of **AlOC-196**.

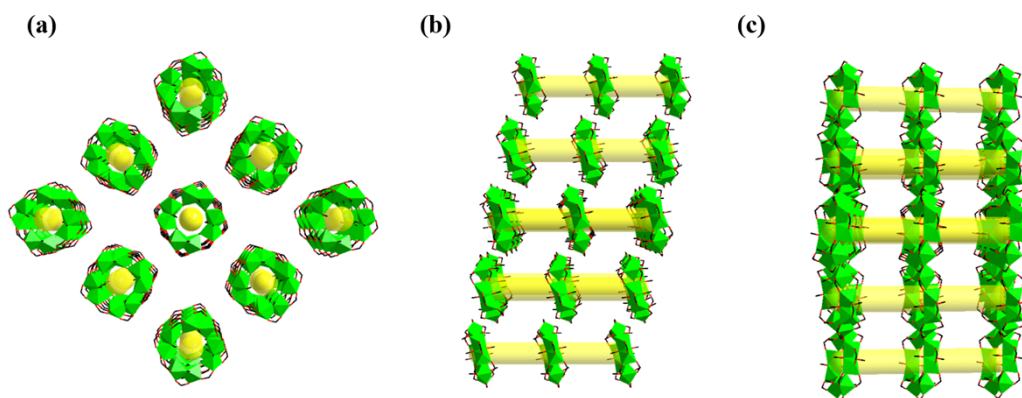**Fig. S2.** The structure of two types of {Al$_2$} units in **AlOC-196**.

Fig. S3. View of the 0D clusters of **AlOC-196** along the a-axis (a), b-axis (b), and c-axis (c).

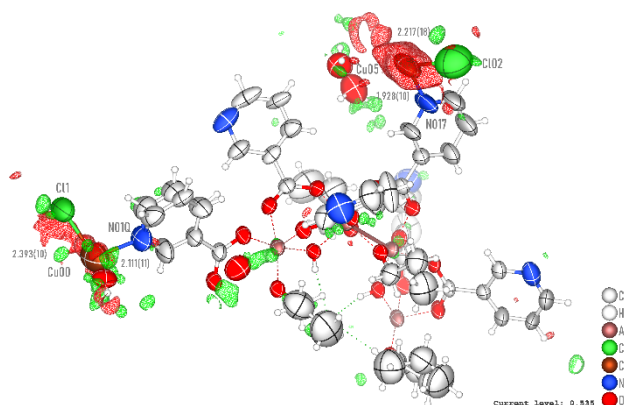# 3. Detailed coordination environment information for 2D network AlOC-197

Fig. S4. Thermal ellipsoid diagram of **AlOC-197**.

Fig. S5. The coordination mode of the bridging nicotinic acid linker. Color code: Al

green; Cu Cu; O red; C black. H atoms are omitted for clarity.
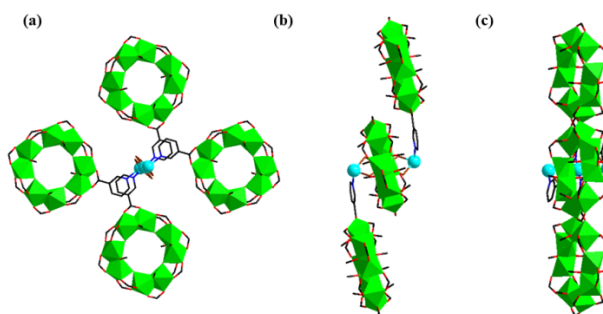
Fig. S6. View of the coordination mode of the 4-connection of $\{Cu_3Cl_4\}$ of **AlOC-197** along the a-axis (a), b-axis (b), and c-axis (c). Some ligands are omitted for clarity.
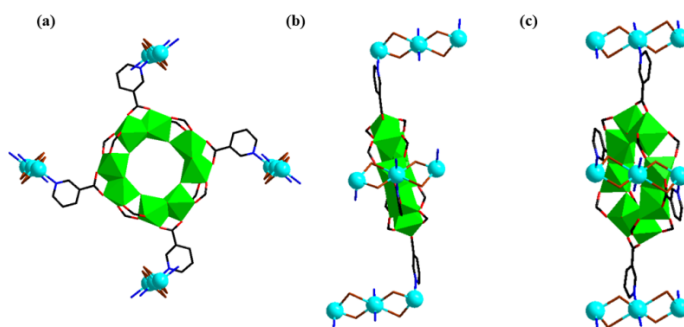

Fig. S7. View of the coordination mode of the $\{Al_8\}$ SBU of **AlOC-197** along the a-axis (a), b-axis (b), and c-axis (c). Some ligands are omitted for clarity.
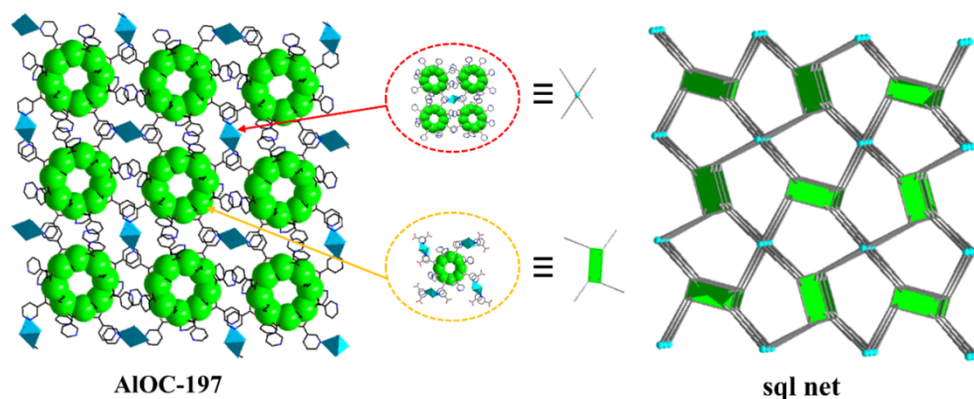

AlOC-197   sql net

Fig. S8. The sql net of **AlOC-197**. (To show the structure of the connections in AlOC-197 more clearly, the $\{Cu_3Cl_4\}$ SBU is simplified as a blue dot, the $\{Al_8\}$ SBU as a

green rectangle, and the nicotinic acid ligand as a gray straight line.)

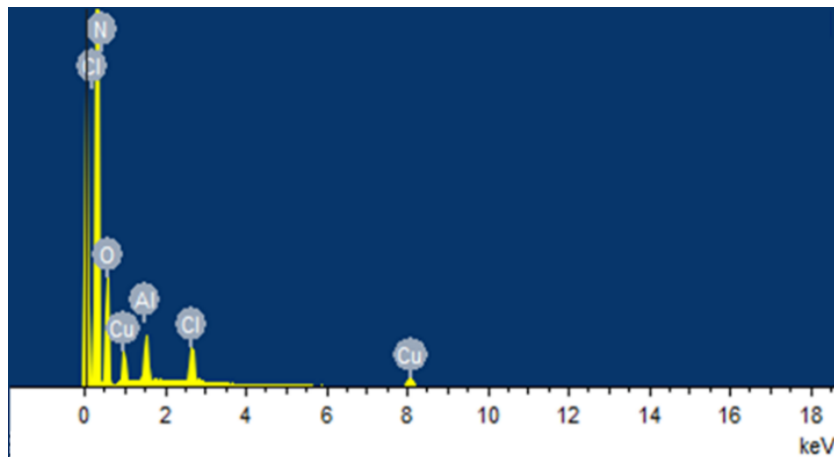## 4. Detailed characterization of bulky crystals AlOC-196 and AlOC-197
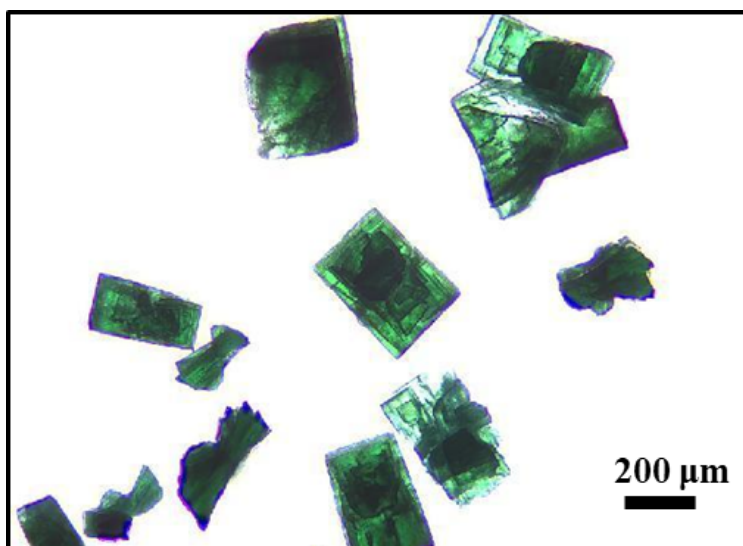

Fig. S9. The EDS spectrum of **AlOC-197**.

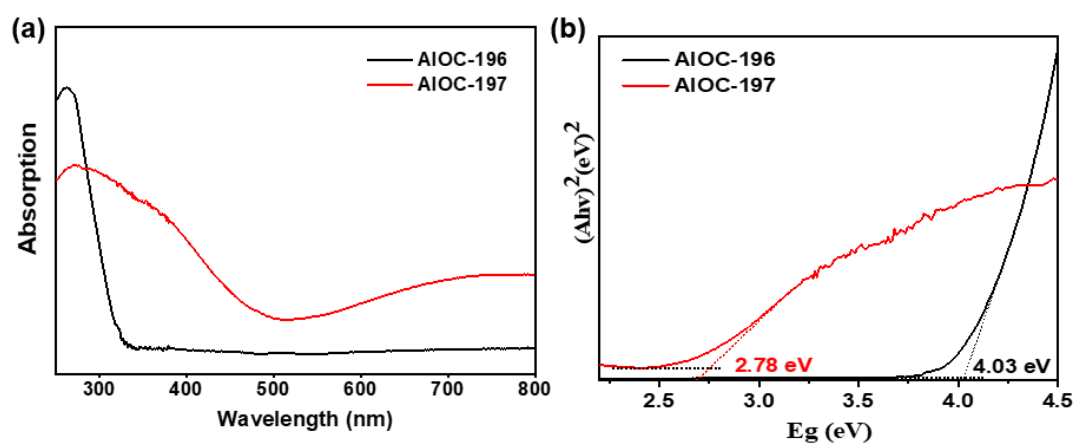**Fig. S10.** The optical photograph of **AlOC-197**.

Fig. S11. Solid-state absorption and band gap analysis of the **AlOC-196** and **AlOC-197**.
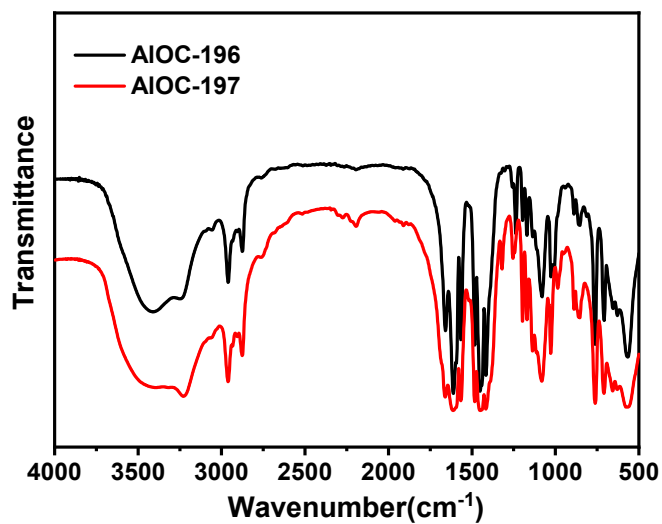

Fig. S12. The FT-IR spectroscopy of **AlOC-196** and **AlOC-197**.

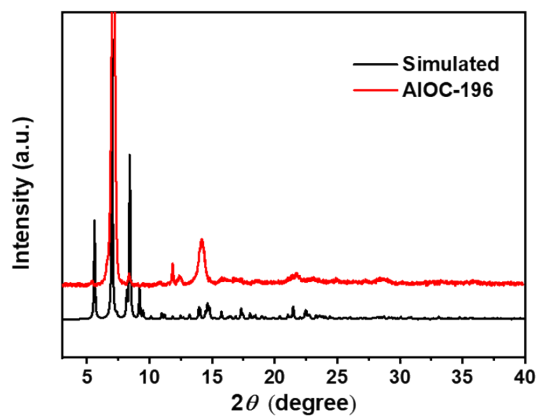## 5. Stability analysis of bulky crystals AlOC-196 and AlOC-197
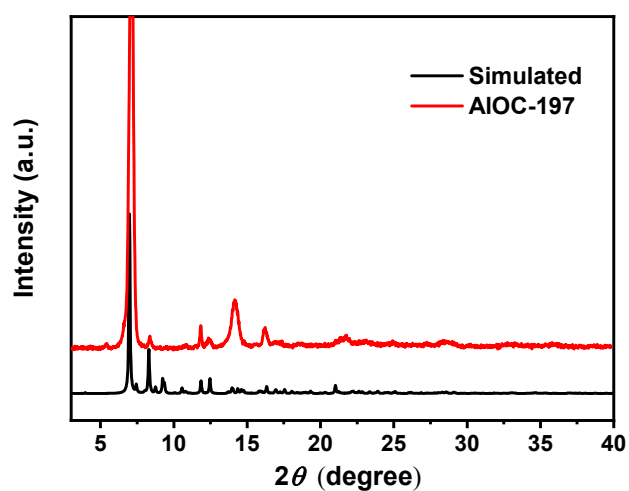
Fig. S13. The PXRD patterns of samples **AlOC-196**.
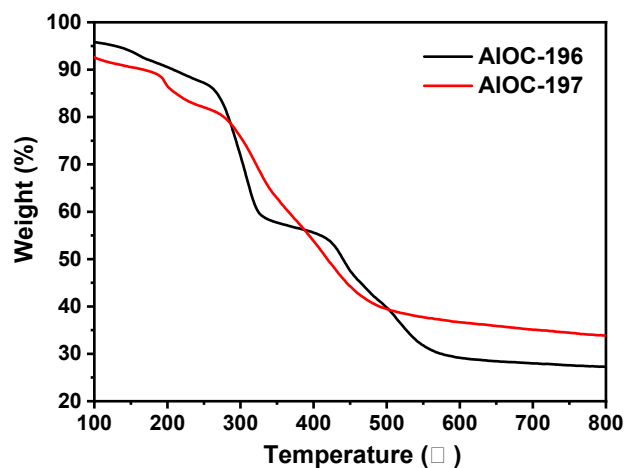

Fig. S14. The PXRD patterns of samples **AlOC-197**.

Fig. S15. The TGA curve of the **AlOC-196** and **AlOC-197**.

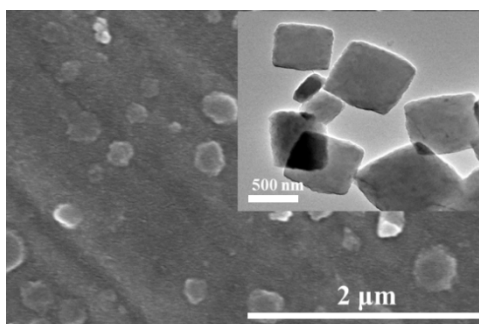## 6. Detailed characterization of AlOC-197 nanosheets

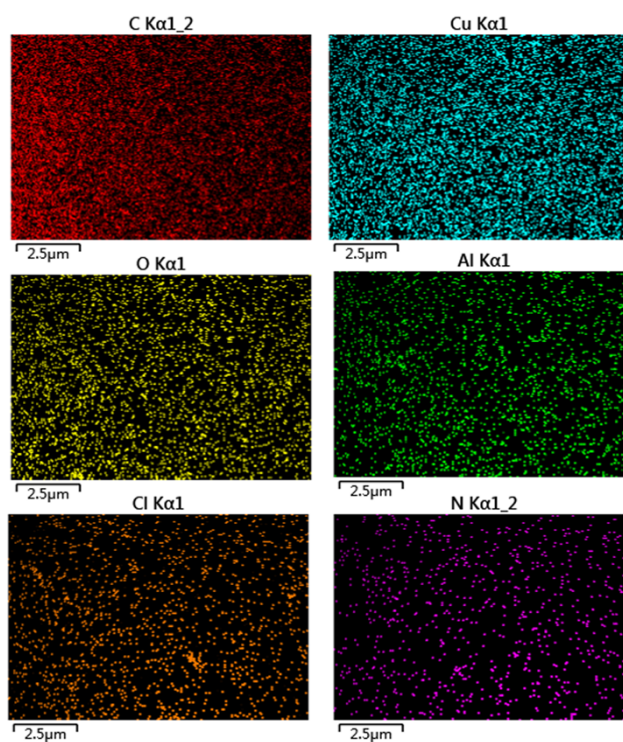**Fig. S16.** The SEM image of **AlOC-197** nanosheets (Inset: TEM image).
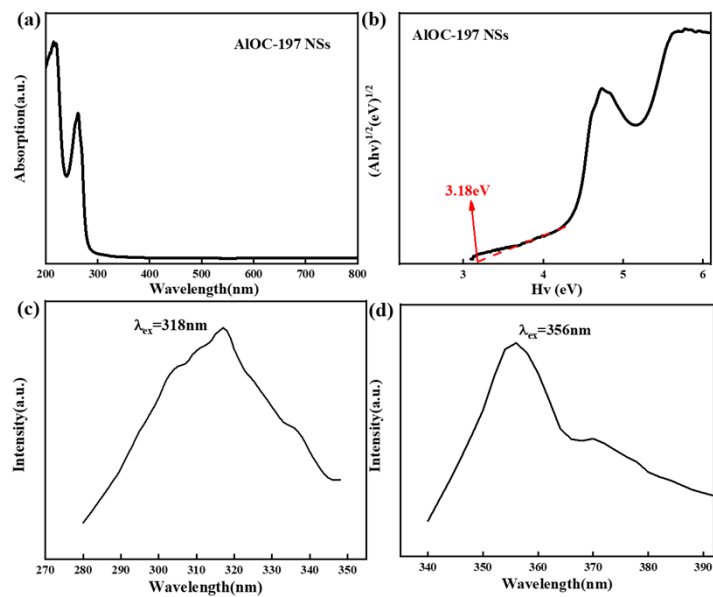

Fig. S17. The EDS spectrum of **AlOC-197** nanosheets.
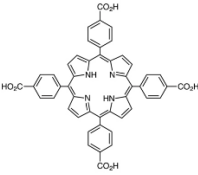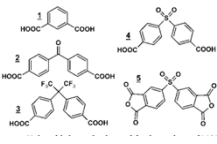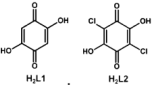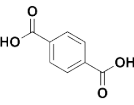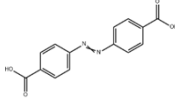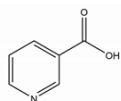
Fig. S18. (a,b) UV-vis absorption, (c) excitation spectra, and (d) emission spectra of **AlOC-197** nanosheets.

7. The summary and comparison of reported typical SBUs of 2D Al-MOFs in previous work

Table S1. The representative 2D Al-MOFs.

MOF	Metal	Linker	SBU	Ref.
Al-TCPP	$Al(NO_3)_3 \cdot 9H_2O$		AlO_6	[1]
CAU-11	$Al(Cl)_3 \cdot 6H_2O$		AlO_6	[2]
CAU-20	$Al(Cl)_3 \cdot 6H_2O$		AlO_6	[3]
CAU-15	$Al_2(SO_4)_3 \cdot 18H_2O$		1D chain	[4]
MIL-129	$Al(NO_3)_3 \cdot 9H_2O$		1D chain	[5]
AlOC-197	$Al(O^iPr)_3$		Al_8 ring	This work

8. Summary of crystallography data for AlOC-196 and AlOC-197

Table S2. Crystallographic data and structure refinement of **AlOC-196** and **AlOC-197**.

Compound	AlOC-196	AlOC-197
Formula	$C_{96}H_{108}Al_8N_{12}O_{38}Cl$	$C_{96}H_{110}Al_8Cl_3Cu_2N_{12}O_{37.25}$
Mr	2257.23	2477.22
Wavelength (Å)	1.54184	1.54184
Crystal system	monoclinic	monoclinic
Space group	$P2_1/c$	$P2_1/c$
a/Å	12.8331(3)	12.5529(7)
b/Å	20.9576(4)	22.1715(11)
c/Å	24.3547(4)	24.0417(9)
α/°	90	90
β/°	100.610(2)	99.549(5)
γ/°	90	90
V/Å^3	6438.2(2)	6598.5(6)
Z	2	2
ρ/g cm^{-3}	1.164	1.247
μ/mm^{-1}	1.420	2.107
$F(000)$	2354.0	2562.0
Collected reflns	27873	19748
Unique reflns (R_{int})	12600 (0.0273)	11376 (0.0652)
GOF on F^2	1.036	1.136
$R_1/wR_2[I>2(I)]$	0.0614/ 0.1832	0.1127/0.2959
CCDC number	2324132	2324133

9. BVS analysis for AlOC-197

Table S3. BVS analysis for Cu of **AlOC-197**.

	Bond	Bond length (Å)	Valence Cu(I)	Valence Cu(II)
Cu05	Cu05-Cl02	2.217	0.38	0.55
	Cu05-Cl02^2	2.217	0.38	0.55
	Cu05-Cl	2.903	0.42	0.56
	Cu05-Cl^2	2.903	0.42	0.56
	Cu05-N017	1.928	0.060	0.087
	Cu05-N017^2	1.928	0.060	0.087
	Sum		1.72	2.39
Cu001	Cu001-Cl1	2.393	0.24	0.35
	Cu001-Cl02^3	2.346	0.27	0.39
	Cu001-N01Q	2.111	0.26	0.34
	Sum		0.77	1.08

10. Third-order nonlinear properties of AlOC-197 nanosheets

Table S4. The NLO parameters for **AlOC-197** nanosheets.

AlOC-197 nanosheets	β ($\times 10^{-11}$ m/W)	$Im\chi^{(3)}$ ($\times 10^{-12}$ esu)	FOM($*10^{-12}$ esu)
10μJ	8.9	2.51	1.96
20μJ	8.1	2.29	1.79
40μJ	10.8	3.05	2.38
60μJ	11.2	3.16	2.47
75μJ	12.8	3.62	2.82

Table S5. The relevant NLO parameters for other low-dimensional materials.

Materials	β ($\times 10^{-11}$m/W)	Im$\chi^{(3)}$ ($\times 10^{-12}$esu)	FOM($*10^{-12}$esu)	Reference
AlOC-197 nanosheets	11.2	3.16	2.47	This work
MoSe$_2$ nanosheets	N/A	1.61	8.72	[6]
Sb nanosheets	10.5	N/A	N/A	[7]
GeSe nanosheets	5.61	0.84×10^{-2}	N/A	[8]
SnSe nanosheets	0.02	1.452×10^{5}	N/A	[9]
C$_{60}$	22.57	8.55	N/A	[10]
BN nanosheets	0.079	0.653	N/A	[11]
CuS nanosheets	11.4	3.36×10^{4}	N/A	[12]

Reference

1. M. Jian, R. Qiu, Y. Xia, J. Lu, Y. Chen, Q.Gu, R. Liu, C. Hu, J. Qu, H. Wang and X. Zhang, *Sci. Adv.*, 2020, **6**.
2. N. Reimer, H. Reinsch, A. K. Inge and N. Stock, *Inorg. Chem.* 2015, **54**, 492−501.
3. H. Halis, A. K. Inge, N. Dehning, T. Weyrich, H. Reinsch, and N. Stock *Inorg. Chem.* 2016, **55**, 7425−7431.
4. H. Reinsch, D. D. Vos, and N. Stock, *Z. Anorg. Allg. Chem.* 2013*, 639, 2785–2789*
5. C. Volkringer, T. Loiseau, T. Devic, G. Férey, D. Popov, M. Burghammer and C. Riekel, *CrystEngComm* 2010, **12**, 3225-3228.
6. H. Pan, H. Chu, Y. Li, S. Zhao and D. Li, *J. Alloys.Compd.*, 2019, **806**, 52-57.
7. L. Zhang, S. Fahad, H.-R. Wu, T.-T. Dong, Z.-Z. Chen, Z.-Q. Zhang, R.-T. Liu, X.-P. Zhai, X.-Y. Li, X. Fei, Q.-W. Song, Z.-J. Wang, L.-C. Chen, C.-L. Sun, Y. Peng, Q. Wang and H.-L. Zhang, *Nano. Horizon.*, 2020, **5**, 1420-1429.
8. J. Mu, Z. Yang, Q. Zhang, X. Yuan, G. Wang, H. Qi, F. Wang and W. Sun, *J. Mater. Sci.*, 2023, **58**, 11527-11538.
9. Y. Ye, Y. Xian, J. Cai, K. Lu, Z. Liu, T. Shi, J. Du, Y. Leng, R. Wei, W. Wang, X. Liu, G. Bi and J. Qiu, *Adv. Opt.Mater.*, 2019, **7**.
10. Y. Chen, T. Bai, N. Dong, F. Fan, S. Zhang, X. Zhuang, J. Sun, B. Zhang, X. Zhang, J. Wang and W. J. Blau, *Prog. Mater. Sci.*, 2016, **84**, 118-157.
11. F. Ma, M. Wang, Y. Shao, L. Wang, Y. Wu, Z. Wang and X. Hao, *J. Mater. Chem. C*, 2017, **5**, 2559-2565.
12. N. Ahmad, A. M. Alshehri, Z. R. Khan, S. A. M. Almahdawi, M. Shkir, P. M. Z. Hasan, A. Alshahrie, F. Khan and A. Al-Ahmed, *Inorg. Chem.Commun.*, 2022, **139**.